

# 12 Aspects of Topological Superconductivity

Manfred Sgrist

Institute for Theoretical Physics

ETH Zürich, Switzerland

## Contents

<b>1</b>	<b>Introduction</b>	<b>2</b>
<b>2</b>	<b>Unconventional superconductivity</b>	<b>2</b>
2.1	Pair wave function . . . . .	2
2.2	Symmetry properties . . . . .	3
<b>3</b>	<b>Topological properties of a two-dimensional chiral superconductor</b>	<b>5</b>
3.1	Nambu space representation . . . . .	5
3.2	Topological invariant – Chern number . . . . .	6
3.3	Symmetry criterion . . . . .	10
<b>4</b>	<b>Edge states in chiral superconductors</b>	<b>11</b>
4.1	Edge states . . . . .	11
4.2	Surface currents . . . . .	14
4.3	Quasiparticle current and thermal Hall effect . . . . .	15
<b>5</b>	<b>Chiral superconductivity in three dimensions</b>	<b>17</b>
<b>6</b>	<b>Topological superconducting phases with TRS</b>	<b>19</b>
6.1	Two-dimensional systems . . . . .	19
6.2	Surface currents and universal properties . . . . .	20
6.3	Three-dimensional systems . . . . .	21
<b>7</b>	<b>Symmetry classification</b>	<b>22</b>
<b>8</b>	<b>Realizations of topological superconducting phases</b>	<b>23</b>
<b>9</b>	<b>Conclusion</b>	<b>24</b>

# 1 Introduction

Superconductivity is undoubtedly one of the most remarkable and enigmatic ground states of electronic matter. At sufficiently low temperature electrons of a metal condense into a coherent state of Cooper pairs and open a single-quasiparticle excitation gap. This has been the notion of the BCS theory of 1957 which counts among the most comprehensive descriptions of many-electron properties in condensed matter physics. While the original BCS theory is based on the simplest intrinsic structure of Cooper pairs, superconductivity appearing in systems with strong electron correlation realizes more complex pair wave states whose internal structure expand the space of superconducting phases and phenomena tremendously. As we will discuss below, we distinguish between *conventional* and *unconventional* superconducting states [1–3]. The former are found in the standard textbook superconductors such as the elemental metals Pb, Al or Nb and many compounds. Unconventional superconductivity, on the other hand, occurs in materials classes like the cuprate high temperature superconductors such as  $\text{YBa}_2\text{Cu}_3\text{O}_7$  and the heavy Fermion compounds represented by  $\text{URu}_2\text{Si}_2$ ,  $\text{UPt}_3$  and  $\text{CeCoIn}_5$ , which all also show strong magnetic correlations [4–7]. An intensely studied case is  $\text{Sr}_2\text{RuO}_4$  whose nature of superconductivity is debated at present [8, 9].

In this lecture we would like to address a special subclass among the unconventional superconductors which display topological properties. The first phases in this class were actually not superconductors, but the neutral superfluid  $^3\text{He}$  whose phases rest on the same Cooper pairing paradigm as all known superconductors.  $^3\text{He}$  has two phases in the absence of a magnetic field, the A-phase and the B-phase, which both have topological properties and distinguish themselves by their symmetry [10]. While the B-phase preserves maximal possible symmetries of the fluid, the A-phase spontaneously violates time reversal symmetry (TRS) and is known as a “chiral superfluid”. Both phases can generate topologically protected edge states, a trade mark of topological insulators. In the following we will put our focus on chiral superconducting phases which break TRS and explain some of the important features and phenomena. We will also touch briefly upon TRS conserving topological superconductors. In this lecture it is expected that the basics of BCS superconductivity are known, but otherwise the technical level will be kept rather low. There are textbooks and numerous review articles which go deeper into technical details [11–14]. Early works by G. Volovik date back more than three decades [15].

## 2 Unconventional superconductivity

### 2.1 Pair wave function

We first address the nature of an unconventional superconductor by analyzing the structure of its ground state and at the same time introduce the standard notations. For simplicity we restrict ourselves here exclusively to systems with a single electronic band whose states are Bloch states  $|\mathbf{k}, s\rangle$  created (annihilated) by the operators  $\hat{c}_{\mathbf{k}s}^\dagger$  ( $\hat{c}_{\mathbf{k}s}$ ). The BCS-like ground state is a coherent state of electron pairs (Cooper pairs) with vanishing total momentum, such that we can define a

pair wavefunction,

$$F_{ss'}(\mathbf{k}) = \langle \hat{c}_{-\mathbf{k}s'} \hat{c}_{\mathbf{k}s} \rangle \quad (1)$$

where  $\langle \dots \rangle$  denotes the expectation value for the ground state or a thermal average, in general. Obviously, the particle number is not conserved as is the essence of a coherent state. The wavefunction is  $2 \times 2$ -matrix in spin space and satisfies the relation  $\hat{F}(\mathbf{k}) = -\hat{F}(-\mathbf{k})^T$  due to the Pauli principle, i.e., the pair wave function is odd under exchange of the two electrons. If time reversal and inversion symmetry are preserved in the normal state, we distinguish the two cases

$$\hat{F}(\mathbf{k}) = \begin{cases} f_0(\mathbf{k}) \hat{\sigma}^0 i \hat{\sigma}^y & \text{with } f_0(\mathbf{k}) = f_0(-\mathbf{k}) \\ \mathbf{f}(\mathbf{k}) \cdot \hat{\boldsymbol{\sigma}} i \hat{\sigma}^y & \text{with } \mathbf{f}(\mathbf{k}) = -\mathbf{f}(-\mathbf{k}) \end{cases} \quad (2)$$

where the upper stands for an even-parity spin-singlet and lower for an odd-parity spin-triplet pairing state, represented by a scalar ( $f_0(\mathbf{k})$ ) and vector ( $\mathbf{f}(\mathbf{k})$ ) wavefunction. Here  $\hat{\boldsymbol{\sigma}}$  denotes the Pauli matrices and  $\hat{\sigma}^0$  the two-dimensional unit matrix.

We distinguish conventional and unconventional Cooper pairing by the sum of  $f_0(\mathbf{k})$  over the Brillouin zone (BZ)

$$I_0 = \sum_{\mathbf{k} \in \text{BZ}} f_0(\mathbf{k}) \quad \text{and} \quad \mathbf{I} = \sum_{\mathbf{k} \in \text{BZ}} \mathbf{f}(\mathbf{k}) \quad (3)$$

which is proportional to the real space on-site amplitude of the pair wavefunction.<sup>1</sup> The notion *conventional* only applies to even parity states with  $I_0 \neq 0$ . All states with  $I_0 = 0$  or  $\mathbf{I} = 0$  are called *unconventional*. Obviously, all odd-parity states are unconventional. The fact that paired electrons avoid to meet on the same position, gives these states an advantage over conventional pairs in systems with strong electron repulsion. In such a case, standard electron-phonon mediated pairing interaction, which is essentially a contact interaction, is ineffective in causing unconventional pairing states and other pairing mechanism yielding longer-ranged interactions are necessary, such as spin fluctuation exchange.

## 2.2 Symmetry properties

Within Landau theory of second-order phase transitions the low-temperature ordered phase is characterized by an order parameter describing the spontaneous symmetry breaking. This order parameter belongs to an irreducible representation of the normal state symmetry group, for superconductivity involving the crystal point group ( $\mathcal{P}$ ), spin rotation ( $SU(2)$ ), and TRS ( $\mathcal{T}$ ) which can be broken in unconventional superconducting states beside  $U(1)$ -gauge symmetry (coherent state). The general pair wave function can be written as a superposition

$$\hat{F}(\mathbf{k}) = \sum_{n=1}^{N_\Gamma} \eta_n \hat{F}_{\Gamma,n}(\mathbf{k}) \quad (4)$$

<sup>1</sup>The real space pair wavefunction is given by the Fourier transform (with  $\Omega$  as the volume)

$$\hat{\Phi}(\mathbf{r}-\mathbf{r}') = \frac{1}{\Omega} \sum_{\mathbf{k} \in \text{BZ}} \hat{F}(\mathbf{k}) e^{i\mathbf{k} \cdot (\mathbf{r}-\mathbf{r}')}$$

where the  $\{\hat{F}_{\Gamma,1}(\mathbf{k}), \dots, \hat{F}_{\Gamma,N_\Gamma}(\mathbf{k})\}$  form the basis set of the irreducible representation  $\Gamma$  of dimension  $N_\Gamma$ , and  $\eta_n$  are complex coefficients. The symmetry operations are most conveniently performed within the notation introduced in Eq. (2), where rotation operations  $g \in \mathcal{P}$  (spin and lattice are tied together through spin-orbit coupling) lead to

$$g \circ \hat{F}(\mathbf{k}) \Rightarrow \begin{cases} g \circ f_0(\mathbf{k}) = f_0(R_g \mathbf{k}) \\ g \circ \mathbf{f}(\mathbf{k}) = R_g \mathbf{f}(R_g \mathbf{k}) \end{cases} \quad (5)$$

with  $R_g$  is the corresponding real space rotation matrix. Inversion yields  $\mathcal{I} \circ f_0(\mathbf{k}) = f_0(-\mathbf{k}) = f_0(\mathbf{k})$  and  $\mathcal{I} \circ \mathbf{f}(\mathbf{k}) = \mathbf{f}(-\mathbf{k}) = -\mathbf{f}(\mathbf{k})$ . Time reversal and  $U(1)$ -operation,  $\mathcal{K}$  and  $\Phi$ , respectively, give

$$\mathcal{K} \circ f_\mu(\mathbf{k}) = f_\mu(\mathbf{k})^* \quad \text{and} \quad \Phi \circ f_\mu(\mathbf{k}) = f_\mu(\mathbf{k})e^{i\phi}. \quad (6)$$

Assuming that a given superconducting phase belongs to a single representation, we can associate its symmetry properties easily with the behavior of the corresponding basis functions. The conventional superconducting phase is in the non-degenerate trivial representation of even parity, constituting the state of highest possible symmetry – only  $U(1)$ -gauge symmetry is broken. Otherwise, in Eq. (3) the sum  $I_0$  would vanish.

A particularly important feature is the *degeneracy*, connected with the dimension  $N_\Gamma$ , because it allows for intriguing phenomena which are not available in conventional superconductors. For a concrete and simple example, we consider here the case of  $N_\Gamma = 2$  which is important for topologically non-trivial superconductors with chiral pairing. For this purpose we look at the tetragonal point group,  $D_{4h}$ , which has two-dimensional irreducible representations  $E_g$  and  $E_u$ , with even and odd parity, respectively. The basis functions reflecting the symmetry operations are in their most simple form

$$\begin{aligned} E_g : \quad & f_{0,\Gamma,x}(\mathbf{k}) = k_z k_x & f_{0,\Gamma,y}(\mathbf{k}) = k_z k_y \\ E_u : \quad & \mathbf{f}_{\Gamma,x}(\mathbf{k}) = \hat{z} k_x & \mathbf{f}_{\Gamma,y}(\mathbf{k}) = \hat{z} k_y \end{aligned} \quad (7)$$

where  $\mathbf{f}$  of the odd parity state is oriented along the  $z$ -axis corresponding to the spin-triplet state with the spin state  $(S, S_z) = (1, 0)$  corresponding to “equal spin” pairing.

Only a discrete set of superpositions of these basis states are stable. The possible superconducting phases for these degenerate pairing state basis can be found using the Landau free energy expansion in the order parameter. The complex coefficients  $\eta_n$  of Eq. (4), which has two components  $\boldsymbol{\eta} = (\eta_x, \eta_y)$ , can play the role of the order parameter. The free energy then contains the following terms,

$$F[\boldsymbol{\eta}] = a(T)|\boldsymbol{\eta}|^2 + b_1|\boldsymbol{\eta}|^4 + \frac{b_2}{2} \{ \eta_x^{*2} \eta_y^2 + \eta_x^2 \eta_y^{*2} \} + b_3 |\eta_x|^2 |\eta_y|^2 \quad (8)$$

which include all independent scalar combinations of  $\boldsymbol{\eta}$  transforming under  $E_{g,u}$  up to 4<sup>th</sup> order. There are only three fourth-order terms. Here  $a(T) = a'(T - T_c)$  (both components have the same critical temperature) and  $b_1, b_2$  and  $b_3$  are real coefficients. All coefficients constitute

material specific input to the theory. Under the constraint that the free energy is bound from below, we find the following three phases

$$\boldsymbol{\eta}_A \propto \begin{Bmatrix} (1, +i) \\ (1, -i) \end{Bmatrix}, \quad \boldsymbol{\eta}_B \propto \begin{Bmatrix} (1, +1) \\ (1, -1) \end{Bmatrix}, \quad \boldsymbol{\eta}_C \propto \begin{Bmatrix} (1, 0) \\ (0, 1) \end{Bmatrix}, \quad (9)$$

which all are two-fold degenerate. The phase *A* is *chiral* and breaks TRS, while the other two are *nematic* and break crystal rotational symmetry. Which of the three phases is realized depends on microscopic details not accessible to our symmetry arguments. A weak-coupling approach yield generally the *A*-phase as most stable as it has least zero nodes. In the following we will focus on this phase, because it includes the best known topologically non-trivial superconducting phase.

### 3 Topological properties of a two-dimensional chiral superconductor

In this section we start out with a superconductor within a two-dimensional or a quasi-two-dimensional metal, where the latter is characterized by having an essentially cylindrical Fermi surface (FS) as we will encounter also in Sect. 5. As mentioned above we restrict to a single band model and assume basic knowledge of the BCS theory.

#### 3.1 Nambu space representation

In a first step we introduce the Nambu representation of the microscopic Hamiltonian in mean field form (up to added constant terms)

$$\mathcal{H}_{\text{mf}} = \frac{1}{2} \sum_{\mathbf{k}} \hat{C}_{\mathbf{k}}^\dagger H_{\mathbf{k}} \hat{C}_{\mathbf{k}} \quad (10)$$

with the Nambu spinor  $\hat{C}_{\mathbf{k}} = (\hat{c}_{\mathbf{k}\uparrow}, \hat{c}_{\mathbf{k}\downarrow}, \hat{c}_{-\mathbf{k}\uparrow}^\dagger, \hat{c}_{-\mathbf{k}\downarrow}^\dagger)^T$  and the Hamiltonian matrix

$$H_{\mathbf{k}} = \begin{pmatrix} \xi_{\mathbf{k}} \hat{\sigma}^0 & \hat{\Delta}_{\mathbf{k}} \\ \hat{\Delta}_{\mathbf{k}}^\dagger & -\xi_{-\mathbf{k}} \hat{\sigma}^0 \end{pmatrix} \quad (11)$$

with  $\xi_{\mathbf{k}}$  as the band energy measured relative the chemical potential  $\mu$  ( $\xi_{\mathbf{k}} = 0$  defines the FS) and the gap function

$$\hat{\Delta}_{\mathbf{k}} = i\hat{\sigma}^y \{ \hat{\sigma}^0 d_0(\mathbf{k}) + \hat{\boldsymbol{\sigma}} \cdot \mathbf{d}(\mathbf{k}) \} = \begin{pmatrix} -d_x(\mathbf{k}) + id_y(\mathbf{k}) & d_z(\mathbf{k}) + d_0(\mathbf{k}) \\ d_z(\mathbf{k}) - d_0(\mathbf{k}) & d_x(\mathbf{k}) + id_y(\mathbf{k}) \end{pmatrix} \quad (12)$$

with  $d_0(\mathbf{k})$  even and  $\mathbf{d}(\mathbf{k})$  odd functions of  $\mathbf{k}$ . The Nambu representation doubles the electronic spectrum by adding the (redundant) hole spectrum. The coherent state corresponds to a hybridization of electrons and holes through the off-diagonal elements  $\hat{\Delta}_{\mathbf{k}}$ , which are connected with the pair wavefunction within mean field theory through the pairing interaction

$$\hat{V} = \frac{1}{2} \sum_{\mathbf{k}, \mathbf{k}'} \sum_{s_1, s_2, s_3, s_4} V_{\mathbf{k}, \mathbf{k}'}^{s_1 s_2 s_3 s_4} \hat{c}_{\mathbf{k} s_1}^\dagger \hat{c}_{-\mathbf{k} s_2}^\dagger \hat{c}_{-\mathbf{k}' s_3} \hat{c}_{\mathbf{k}' s_4} \cdot \quad (13)$$

The relation is given by

$$\Delta_{\mathbf{k}ss'} = - \sum_{\mathbf{k}'} \sum_{\tilde{s}, \tilde{s}'} V_{\mathbf{k}, \mathbf{k}'}^{ss' \tilde{s} \tilde{s}'} F_{\tilde{s}' \tilde{s}}(\mathbf{k}) \quad (14)$$

such that the symmetry properties of the  $\hat{\Delta}_{\mathbf{k}}$  and  $\hat{F}(\mathbf{k})$  are identical.

The Hamiltonian in Eq. (10) with (11) yields the spectrum

$$E_{\mathbf{k}} = \sqrt{\xi_{\mathbf{k}}^2 + |\Delta_{\mathbf{k}}|^2} \quad \text{with} \quad |\Delta_{\mathbf{k}}|^2 = \frac{1}{2} \text{Tr} \hat{\Delta}_{\mathbf{k}}^\dagger \hat{\Delta}_{\mathbf{k}} \quad (15)$$

for the Bogoliubov quasiparticles  $\hat{A}_{\mathbf{k}} = (\hat{a}_{\mathbf{k}\alpha}, \hat{a}_{\mathbf{k}\beta}, \hat{a}_{-\mathbf{k}\alpha}^\dagger, \hat{a}_{-\mathbf{k}\beta}^\dagger)$  obtained by the unitary transformation

$$\hat{C}_{\mathbf{k}} = U_{\mathbf{k}} \hat{A}_{\mathbf{k}} \quad \text{with} \quad U_{\mathbf{k}} = \begin{pmatrix} \hat{u}_{\mathbf{k}} & \hat{v}_{\mathbf{k}} \\ \hat{v}_{-\mathbf{k}}^* & \hat{u}_{-\mathbf{k}}^* \end{pmatrix} \quad (16)$$

with  $U_{\mathbf{k}} U_{\mathbf{k}}^\dagger = 1$ . We derive  $U_{\mathbf{k}}$  through the condition

$$U_{\mathbf{k}}^\dagger H_{\mathbf{k}} U_{\mathbf{k}} = \begin{pmatrix} E_{\mathbf{k}} \hat{\sigma}^0 & 0 \\ 0 & -E_{-\mathbf{k}} \hat{\sigma}^0 \end{pmatrix}. \quad (17)$$

Note that  $\hat{u}_{\mathbf{k}}$  and  $\hat{v}_{\mathbf{k}}$  constitute wave functions of the electron and the hole-like components of the quasiparticles, respectively, as can be seen from

$$\hat{u}_{\mathbf{k}} = \frac{1}{\sqrt{2}} \sqrt{1 + \frac{\xi_{\mathbf{k}}}{E_{\mathbf{k}}}}, \quad \hat{v}_{\mathbf{k}} = -\frac{\hat{\Delta}_{\mathbf{k}}}{\sqrt{2}|\Delta_{\mathbf{k}}|} \sqrt{1 - \frac{\xi_{\mathbf{k}}}{E_{\mathbf{k}}}}. \quad (18)$$

### 3.2 Topological invariant – Chern number

We now turn to the chiral  $A$ -phase we introduced above and restrict ourselves to the odd parity case, because the even-parity state cannot be realized in a purely two-dimensional system as it involves  $k_z$ -dependence, indicating extensions of Cooper pairs along the  $z$ -axis. Because it will be useful later, we consider here a tight-binding model on a square lattice with a simple nearest-neighbor hopping dispersion

$$\xi_{\mathbf{k}} = -2t(\cos k_x + \cos k_y) - \mu \quad (19)$$

where  $t$  is the hopping matrix element and the lattice constant is unity. The Cooper pairs shall originate from a nearest-neighbor pairing interaction, which leads to the pair wave function and the gap function

$$\mathbf{f}^\pm(\mathbf{k}) = F_0 \hat{\mathbf{z}} (\sin k_x \pm i \sin k_y) \quad \text{and} \quad \mathbf{d}^\pm(\mathbf{k}) = \Delta_0 \hat{\mathbf{z}} (\sin k_x \pm i \sin k_y) \quad (20)$$

transforming within  $E_u$  of the tetragonal point group. It is easy to see that for this gap structure using Eq. (12) the gap matrix  $H(\mathbf{k})$  in Eq. (11) can be decomposed into two disconnected parts with two-dimensional Hamiltonian matrices,

$$h(\mathbf{k}) = \begin{pmatrix} \xi_{\mathbf{k}} & d_z(\mathbf{k}) \\ d_z^*(\mathbf{k}) & -\xi_{\mathbf{k}} \end{pmatrix} = \mathbf{h}_{\mathbf{k}} \cdot \hat{\boldsymbol{\tau}} \quad (21)$$

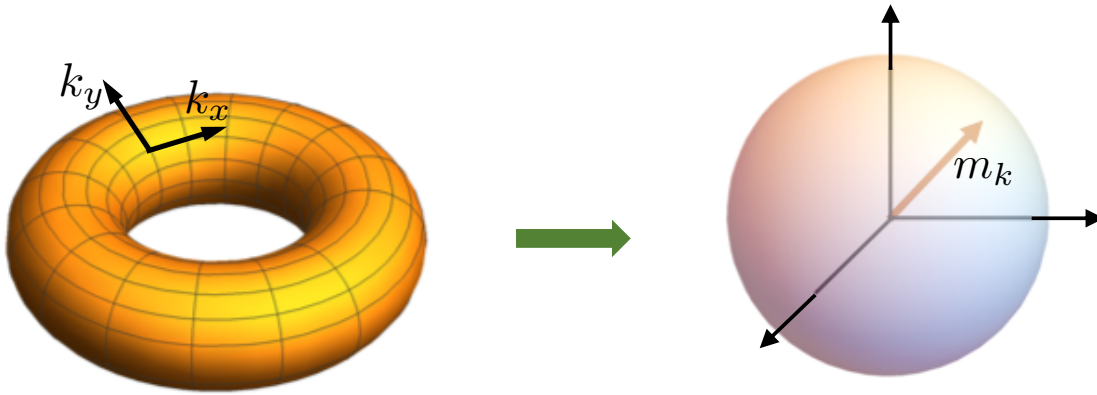


**Fig. 1:** Mapping from the Brillouin zone to the unit sphere: The representation of the Hamiltonian  $\mathbf{h}_{\mathbf{k}}$  as a unit vector  $\mathbf{m}_{\mathbf{k}} = \mathbf{h}_{\mathbf{k}}/|\mathbf{h}_{\mathbf{k}}|$  allows us to map the two-dimensional BZ in  $\mathbf{k}$ -space to a unit sphere.

corresponding to the spinors  $(\hat{c}_{\mathbf{k}\uparrow}, \hat{c}_{-\mathbf{k}\downarrow}^\dagger)$  and  $(\hat{c}_{\mathbf{k}\downarrow}, \hat{c}_{-\mathbf{k}\uparrow}^\dagger)$ , where  $\tau$  are Pauli matrices for the particle-hole space. Note that this can be considered now a spinless subspaces. The three-dimensional vector

$$\mathbf{h}_{\mathbf{k}} = [\text{Im}(d_z(\mathbf{k})), \text{Re}(d_z(\mathbf{k})), \xi_{\mathbf{k}}] \quad (22)$$

is a mapping of the two-dimensional BZ (torus) to a sphere with unit vector  $\mathbf{m}_{\mathbf{k}} = \mathbf{h}_{\mathbf{k}}/|\mathbf{h}_{\mathbf{k}}|$  (Fig. 1). With  $\mathbf{m}_{\mathbf{k}}$  we define

$$\Omega_{\mathbf{k}}^z = \frac{1}{2} \mathbf{m}_{\mathbf{k}} \cdot [\partial_{k_x} \mathbf{m}_{\mathbf{k}} \times \partial_{k_y} \mathbf{m}_{\mathbf{k}}] \quad (23)$$

which is known as the  $z$ -component of the Berry curvature  $\Omega_{\mathbf{k}}$ . We use now  $\Omega_{\mathbf{k}}^z$  to define a *topological invariant*, the *Chern number*, to characterize the chiral state. The Chern number  $C$  is obtained from  $\Omega_{\mathbf{k}}^z$  by an integral over the BZ

$$N_C = 2\pi \int_{\text{BZ}} \frac{d^2k}{(2\pi)^2} \Omega_{\mathbf{k}}^z \quad (24)$$

and is an integer for a topologically non-trivial state. Geometrically this corresponds to (half of) the area element on the sphere, such that the integral (24) results in the number of times  $\mathbf{m}_{\mathbf{k}}$  wraps around the sphere when  $\mathbf{k}$  covering the (torus of) the BZ.

The calculation of  $C$  in this way looks rather tedious. Fortunately, there is a considerably simpler way to determine the Chern number which relies on the knowledge of the gap function on the FS:

$$N_C = \frac{1}{2\pi} \oint_{\text{FS}} d\mathbf{k} \cdot \nabla_{\mathbf{k}} \arg[d_z(\mathbf{k})] \quad (25)$$

which corresponds to the non-trivial phase winding of the gap function (analogous for the pair wavefunction) around the FS. It is rather easy to see that for  $\mu < 0$  the FS is closed around the BZ center and the phase of  $d_z(\mathbf{k})$  acquires a winding of  $2\pi$  going around the FS in positive

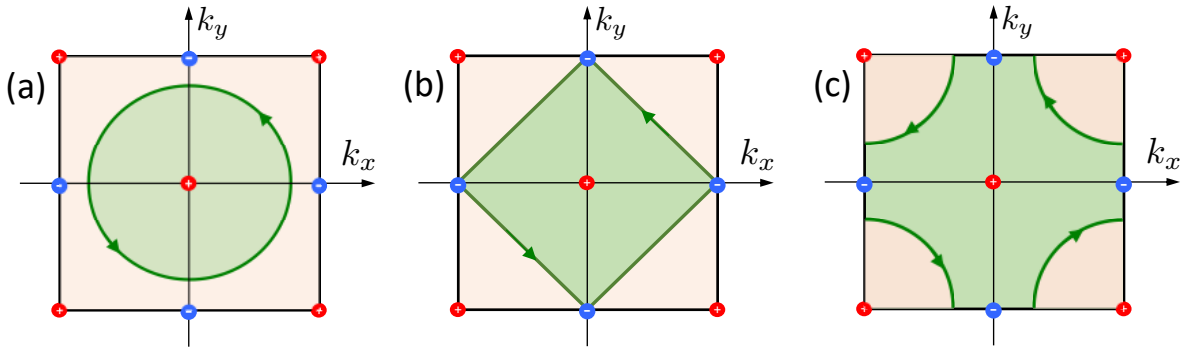


**Fig. 2:** Charges of the gap function  $d_z^+(\mathbf{k})$  in the first BZ. The Chern charges are +1 for the red circles and  $-1$  for the blue points. The Chern number is obtained from Eq. (25) by counting the charge which is encircled by the Fermi surface as a path running in the positive orientation. (a) Below half filling: FS closed around center of the BZ and has  $C = +1$ ; (b) At half filling: the gap function vanishes on the FS at the blue points on the BZ boundary, such that Eq. (25) is not defined; (c) Above half filling: the FS closes around a red corner point of the BZ, which leads to  $C = -1$  when considering that effective path orientation is negative. Note that (b) is the point of a Lifshitz transition from an electron- to a hole-like FS, which is at the same time a topological transition between different Chern numbers, where the gap vanishes.

direction for the gap function in Eq. (20), with  $d_z^+(\mathbf{k}) = \Delta_0(\sin k_x + i \sin k_y)$ . The gap function  $d_z^-(\mathbf{k})$  yields a winding  $-2\pi$ . The sign of  $N_C$  indicates the sign of chirality.

A further convenient feature of the gap function is the appearance of zeros in the BZ or boundary. Because the gap function is periodic in  $\mathbf{k}$ -space we find for the odd-parity state

$$d_z(\mathbf{k}) = -d_z(-\mathbf{k}) = -d_z(-\mathbf{k} + \mathbf{G}) \quad (26)$$

where  $\mathbf{G}$  is a reciprocal lattice vector. If the condition  $\mathbf{k} = -\mathbf{k} + \mathbf{G}$  is satisfied,  $d_z(\mathbf{k}) = 0$ , which is in the give case true for the four inequivalent points  $\mathbf{K}_{1,\dots,4} = (0, 0), (\pi, 0), (0, \pi), (\pi, \pi)$ . We can attribute these zeros a charge corresponding to a winding number.

$$d_z(\mathbf{k} = \mathbf{K}_n + \mathbf{q}) = \Delta_0 q e^{iQ_n \theta_q} \quad (27)$$

with  $Q_1 = Q_4 = +1$  and  $Q_2 = Q_3 = -1$  for  $d_z^+(\mathbf{k})$  (see Fig. 2). The total charge vanishes,  $\sum_{n=1}^4 Q_n = 0$ . These ‘‘Chern charges’’ are very handy to determine the Chern number through Eq. (25) by examining which charges are encircled in which way. In Fig. 2 we consider three cases of band filling assuming a simple tight-binding model with nearest-neighbor hopping with  $\xi_k$  given in Eq. (19). The case (a) displays a simple electron-like FS ( $\mu < 0$ ) which encircles the charge  $Q_1$  at the BZ center in a positive orientation (arrows). Note we always define ‘‘positive orientation’’ with respect to BZ center. In case (c) the FS ( $\mu > 0$ ) is hole-like, going around the charge  $Q_4$  at the BZ corner. We can calculate  $C$  by shifting the BZ in a way to make  $\mathbf{K}_4$  the center which, however, leaves the orientation of encircling negative and leads to  $C = -1$ . On the other hand, we may stick with Fig. 2(c) and follow the path around the BZ center, which consists of the disconnected green FS lines and join them by a path along the BZ boundary

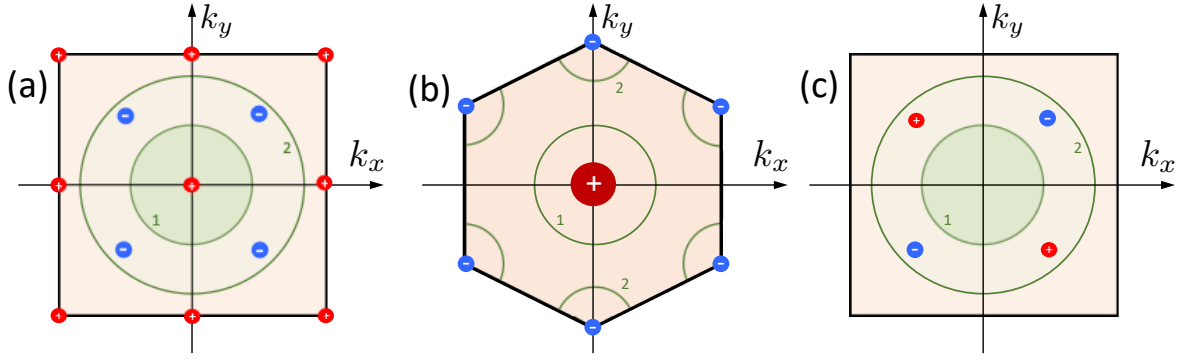


**Fig. 3:** Charges of the various gap functions in the first BZ. (a) Next-nearest neighbor pairing with the gap function  $d_z^+(\mathbf{k})$  of Eq. (29) has  $N_C = +1$  for FS 1 and  $C = -3$  for FS 2. (b) Chiral  $d$ -wave state,  $d_0^\pm(\mathbf{k})$  of Eq. (30) in a hexagonal system has a charge  $Q_1 = 2$  at the BZ center and  $Q_{2,3} = -1$  at the BZ corners for positive chirality. (c)  $s+id$ -wave state of Eq. (31) which has four zeros whose charges cancel to zero for all Fermi surfaces of tetragonal crystal symmetry.

passing through the (blue) charges at  $\mathbf{K}_2$  and  $\mathbf{K}_3$ . In this way we get the Chern number by taking each of the four charge contributions at these BZ boundaries only half, as they are cut. This then yields a full contribution from the charge at the center and four halves from the BZ boundary

$$N_C = +1 + \frac{1}{2}(-4) = -1 \quad (28)$$

consistent with the other view point considering only the charge at  $\mathbf{K}_4$ . The case (b) of half filling ( $\mu=0$ ) corresponds to the Lifshitz transition between the electron- and hole-like FS and leads to a zero in the gap functions,  $d_z(\mathbf{K}_{2,3})=0$ . Here, the Chern number jumps discontinuously and we encounter a topological transition. In Fig. 2 we considered a state with one chirality,  $d_z^+(\mathbf{k}) = \Delta_0(\sin k_x + i \sin k_y)$  which changes under time reversal operation to  $d_z^-(\mathbf{k}) = \Delta_0(\sin k_x - i \sin k_y)$  with all the charges switching sign.

Larger Chern numbers can be obtained by alternative pairing states, e.g., for Cooper pairing of electrons on next-nearest neighbor sites in a square lattice, which lead to a gap function

$$d_z^\pm(\mathbf{k}) = \Delta_0(\cos k_y \sin k_x \pm i \cos k_x \sin k_y). \quad (29)$$

This state belongs to the same representation  $E_u$  as (20), but is different in terms of topology reflected by the Chern number. This gap functions has additional zeros in the BZ besides the ones found above,  $\mathbf{K}_{1,\dots,4}$ . They lie at the four points  $\mathbf{K}_{5,\dots,8} = \frac{\pi}{2}(\pm 1, \pm 1), \frac{\pi}{2}(\pm 1, \mp 1)$ . The charges rearrange:  $Q_{1,\dots,4} = \pm 1$  and  $Q_{5,\dots,8} = \mp 1$  for  $d_z^\pm$  in Eq. (29). Again the total charge vanishes. We encounter here also Chern numbers of  $N_C = \mp 3$  for the electron-like FS 2 enclosing the inner five zeros (see Fig. 3(a)).

Another case is the so-called chiral  $d$ -wave state which is an even-parity spin singlet pairing state. The two necessary components of the basis functions,  $k_x^2 - k_y^2$  and  $k_x k_y$ , are not degenerate in the tetragonal system, but only in a lattice of hexagonal symmetry with point group  $D_{6h}$  where they belong to the two-dimensional representation  $E_{2u}$ . Considering here also a nearest-

neighbor type of pairing state (on a triangular lattice) we obtain a gap function of the form

$$d_0^\pm(\mathbf{k}) = \Delta_0 \sum_{n=1}^3 e^{\pm i 2\pi n/3} \cos(\mathbf{k} \cdot \mathbf{T}_n) \quad (30)$$

with  $\mathbf{T}_1 = (0, 1)$ ,  $\mathbf{T}_2 = (\sqrt{3}/2, -1/2)$  and  $\mathbf{T}_3 = (-\sqrt{3}/2, -1/2)$ . We find zeros at the BZ center and corners,  $\mathbf{K}_1 = (0, 0)$  and  $\mathbf{K}_{2,3} = (0, 1), (\sqrt{3}/2, 1/2)$ , respectively, as shown in Fig. 3(b). The corresponding charges are  $Q_1 = \pm 2$  and  $Q_{2,3} = \mp 1$  ensuring again that the total sum vanishes. The electron-like FS (1) as well as the hole-like FS (2) would, therefore, have  $N_C = \pm 2$ . There is no topological phase transition possible at the Lifshitz transition, since the FS never passes through a gap zero going from FS 1 to FS 2.

Finally we would like to introduce an example of a superconducting phase with broken TRS which is not chiral. This is the well-known  $s + i d_{x^2-y^2}$ -wave state. In the tetragonal crystal lattice the two constituents are not degenerate, as they belong to different one-dimensional representations,  $A_{1g}$  and  $B_{1g}$ . So we assume that for some coincidence both states are competitive, although they may have different strength and also different critical temperatures (superconducting double transition). We consider this state built up from nearest-neighbor pairing,  $d_{0,s}(\mathbf{k}) = \cos k_x + \cos k_y$  also known as extended  $s$ -wave state, and  $d_{0,d}(\mathbf{k}) = \cos k_x - \cos k_y$ . This leads to

$$d_0(\mathbf{k}) = \Delta_s (\cos k_x + \cos k_y) \pm i \Delta_d (\cos k_x - \cos k_y) \quad (31)$$

which has zeros at  $\mathbf{K}_{1,2} = \pm \frac{\pi}{2}(1, 1)$  and  $\mathbf{K}_{3,4} = \pm \frac{\pi}{2}(1, -1)$  whose charges are opposite,  $Q_{1,2} = \pm 1$  and  $Q_{3,4} = \mp 1$  such that the Chern number by symmetry vanishes always, as in Fig. 3(c) for both typical FS (1 and 2).

Note that due to the fact that we have used the reduced Hamiltonian in the discussion following Eq. (21) we should include the spin degeneracy in the Chern number, such that  $N_C$  is multiplied by a factor 2, in general.

### 3.3 Symmetry criterion

Whether an unconventional pairing state is chiral or not can be decided also simply by considering a rather simple symmetry property. As we mentioned before, the ideal condition to get a TRS breaking state is found when the pair wave function belongs to a degenerate irreducible representation of the crystal point group. The chiral superconducting state has a chiral axis which is in the case considered above the  $z$ -axis. Looking at the most simple form of a chiral state,  $k_x \pm i k_y$ , we recognize the spherical harmonic  $Y_{1,\pm 1}(\mathbf{k})$  which corresponds to an angular momentum  $L_z = \pm \hbar$ . In any point group the angular momentum can be associated with irreducible representations  $\Gamma_L$ . In a chiral superconducting state we may attach a net ‘‘angular momentum’’ with the Cooper pair, e.g.,

$$\langle \mathbf{L} \rangle = \left\langle \text{Tr}(\hat{\Delta}_{\mathbf{k}}^\dagger(\mathbf{k} \times \nabla_{\mathbf{k}}) \hat{\Delta}_{\mathbf{k}}) \right\rangle_{BZ} \quad (32)$$

where  $\langle \cdots \rangle_{BZ}$  is an average over the BZ. The symmetry related criterion for a finite  $\langle \mathbf{L} \rangle$  is that the decomposition of  $\Gamma \otimes \Gamma_L \otimes \Gamma$  includes the trivial representation where  $\Gamma$  is the representation

of the pairing state. For the point group  $D_{4h}$  the angular momentum parallel to  $z$ -axis belongs to the  $A_{2g}$ , such that for the chiral  $p$ -wave order parameter in  $E_u$  follows

$$E_u \otimes A_{2g} \otimes E_u = A_{1g} \oplus A_{2g} \oplus B_{1g} \oplus B_{2g} \quad (33)$$

which includes the trivial representation  $A_{1g}$ . Thus, it is possible to construct a chiral pairing state within the representation  $E_u$  of  $D_{4h}$ . The same is true for the representation  $E_{2g}$  in  $D_{6h}$ . On the other hand, the  $s+id$  state is composed of  $A_{1g}$  and  $B_{1g}$  in  $D_{4h}$  and

$$(A_{1g} \oplus B_{1g}) \otimes A_{2g} \otimes (A_{1g} \oplus B_{1g}) = A_{2g} \oplus A_{2g} \oplus B_{2g} \oplus B_{2g} \quad (34)$$

which does not contain  $A_{1g}$ . Thus we cannot form a chiral state from order parameters in these two representations. Interestingly, uniaxial deformation along the axis  $[110]$  would change the condition, reducing the symmetry to  $D_{2h}$  with the corresponding representations  $A_{1g}$  and  $B_{1g}$ . But now the  $L_z$  is also in the representation  $B_{1g}$  and the decomposition within the point group  $D_{2h}$  includes the trivial representation. Returning back to the Chern number, we see in Fig. 3(c) the deformation may change the Fermi surface in way (elliptically elongated along  $[1, 1]$  and squeezed  $[1, -1]$ ) such that only the zeros of charges of the same sign are encircled.

## 4 Edge states in chiral superconductors

In the context of topological phases often the concept of bulk-edge correspondence is mentioned [12, 13]. In chiral superconductors this manifests itself in the presence of chiral quasiparticle modes at the surface with energies below the bulk gap. There is a relation between the Chern number and the basic structure of the edge states as we will point out below, after discussing a specific case. In this section we will also analyze a few physical properties connected with these surface modes.

### 4.1 Edge states

One of the simplest cases to discuss the structure of edge states is a chiral  $p$ -wave state. For this purpose we consider the Bogoliubov-de Gennes equation which allows us to analyze inhomogeneous superconducting phases and local excitation spectra. We will work here with the reduced particle-hole space in the two-spinor representation as given in Eq. (21). To illustrate the edge states it is sufficient to use the Andreev approximation where we focus on the momentum range very close to the FS and separate the fast spatial dependence due to the Fermi wave vector from the slow ones:  $\xi_{\mathbf{k}} \approx \hbar \mathbf{v}_F \cdot (\mathbf{k} - \mathbf{k}_F)$  (see for example Ref. [16]). In a real space formulation this leads to the differential equations

$$\begin{pmatrix} \hbar \mathbf{v}_F \cdot (i \nabla - \mathbf{k}_F) & \Delta_{\mathbf{k}_F} \\ \Delta_{\mathbf{k}_F}^* & -\hbar \mathbf{v}_F \cdot (i \nabla - \mathbf{k}_F) \end{pmatrix} \begin{pmatrix} u_{\mathbf{k}_F}(\mathbf{r}) \\ v_{\mathbf{k}_F}(\mathbf{r}) \end{pmatrix} = E \begin{pmatrix} u_{\mathbf{k}_F}(\mathbf{r}) \\ v_{\mathbf{k}_F}(\mathbf{r}) \end{pmatrix} \quad (35)$$

where  $u_{\mathbf{k}_F}(\mathbf{r})$  and  $v_{\mathbf{k}_F}(\mathbf{r})$  are the electron and hole component of the wave function, respectively, of the stationary eigenstates. These eigenstates are labeled by the Fermi momenta  $\mathbf{k}_F$

indicating the direction of a quasi-classical trajectory of motion, characteristic to the Andreev approximation. With this we can introduce the field operators like

$$\hat{\Psi}(\mathbf{r}) = \sum_{\mathbf{k}_F} \left( \hat{a}_{\mathbf{k}_F} u_{\mathbf{k}_F}(\mathbf{r}) + \hat{a}_{-\mathbf{k}_F}^\dagger v_{\mathbf{k}_F}(\mathbf{r}) \right) \quad (36)$$

where  $(\hat{a}_{\mathbf{k}_F}, \hat{a}_{-\mathbf{k}_F}^\dagger)$  are (spinless) Bogoliubov quasi particle operators. We locate the surface at  $x=0$  (normal vector parallel to  $x$ -axis) and assume specular scattering. Then we can take the ansatz for the wave function

$$\begin{pmatrix} u_{\mathbf{k}_F}(\mathbf{r}) \\ v_{\mathbf{k}_F}(\mathbf{r}) \end{pmatrix} = b_1 \begin{pmatrix} A_{\mathbf{k}_F+}^+ \\ r_{\mathbf{k}_F+} A_{\mathbf{k}_F+}^- \end{pmatrix} e^{+iq_x x + i\mathbf{k}_F+ \cdot \mathbf{r}} + b_2 \begin{pmatrix} r_{\mathbf{k}_F-}^* A_{\mathbf{k}_F-}^- \\ A_{\mathbf{k}_F-}^+ \end{pmatrix} e^{-iq_x x + i\mathbf{k}_F- \cdot \mathbf{r}} \quad (37)$$

with the boundary condition that the wave function vanishes at the surface,  $x=0$  as can be achieved with the proper choice of  $b_{1,2}$ . Moreover,

$$\int_0^\infty dx \int_0^L dy \left( |u_{\mathbf{k}_F}(\mathbf{r})|^2 + |v_{\mathbf{k}_F}(\mathbf{r})|^2 \right) = 1 \quad (38)$$

where periodic boundary condition can be assume along  $y$ -direction for a system of length  $L$ . The parameters in Eq. (37) are  $A_{\mathbf{k}_F\pm}^\pm = [E \pm \sqrt{E^2 - |\Delta_{\mathbf{k}_F}|^2}]^{1/2}$ ,  $\mathbf{k}_{F\pm} = k_F (\pm \cos \theta_{\mathbf{k}_F}, \sin \theta_{\mathbf{k}_F})$ ,  $r_{\mathbf{k}_F} = \Delta_{\mathbf{k}_F}^* / |\Delta_{\mathbf{k}_F}|$ , and  $iq_x = \pm \sqrt{E^2 - |\Delta_{\mathbf{k}_F}|^2} / \hbar v_{F_x}$  ( $|q_x| \ll k_F$ ). Within the Andreev approximation the continuous energy spectrum of the extended quasiparticle state is given by  $E = \pm \sqrt{(\hbar v_F q_x)^2 + |\Delta_{\mathbf{k}_F}|^2}$ . However, there are also states with subgap energies ( $|E| < |\Delta_{\mathbf{k}_F}|$ ) which are bound states at the surface, called *Andreev bound states*. Their energy is obtained by solving the equation

$$r_{\mathbf{k}_F+} r_{\mathbf{k}_F-}^* = \frac{E + \sqrt{E^2 - |\Delta_{\mathbf{k}_F}|^2}}{E - \sqrt{E^2 - |\Delta_{\mathbf{k}_F}|^2}} \Rightarrow E = E_{k_y} = \text{Im} [\Delta_{\mathbf{k}_F}] \Big|_{\mathbf{k}_F \cdot \hat{\mathbf{y}} = k_y} \quad (39)$$

where we use the momentum  $k_{F_y}$  parallel to the surface to label the dispersion as we assume translational invariance along  $y$ -direction. Note that the expression  $E_{k_y} = \text{Im} [\Delta_{\mathbf{k}_F}]$  has to be used with care and is only valid as such for states with  $|N_C|=1$ . For higher Chern numbers the solution of Eq. (39) has to take the winding of the gap function properly into account (see Fig. 4(c) for the example of  $N_C = -3$ ).

We introduce the electron operator  $\hat{\phi}_{k_y}$  specifically for the edge state,

$$\hat{\gamma}_{k_y} = \int d^2 r \left( \hat{\phi}_{k_y} u_{\mathbf{k}_F}^*(\mathbf{r}) - \hat{\phi}_{-k_y}^\dagger v_{\mathbf{k}_F}^*(\mathbf{r}) \right) \quad \text{and} \quad \hat{\gamma}_{-k_y}^\dagger = \int d^2 r \left( \hat{\phi}_{-k_y}^\dagger u_{\mathbf{k}_F}(\mathbf{r}) - \hat{\phi}_{k_y} v_{\mathbf{k}_F}(\mathbf{r}) \right) \quad (40)$$

which then lead to the edge state Hamiltonian,

$$\mathcal{H}_{\text{sf}} = \sum_{k_y} E_{k_y} \hat{\gamma}_{k_y}^\dagger \hat{\gamma}_{k_y}. \quad (41)$$

The same spectrum we obtain also for the other part of the original Hamiltonian, so that we could label  $\hat{\gamma}_{k_y}$  additionally with a spin index. Note that for the zero-energy mode ( $E_{k_y=0}=0$ ) we

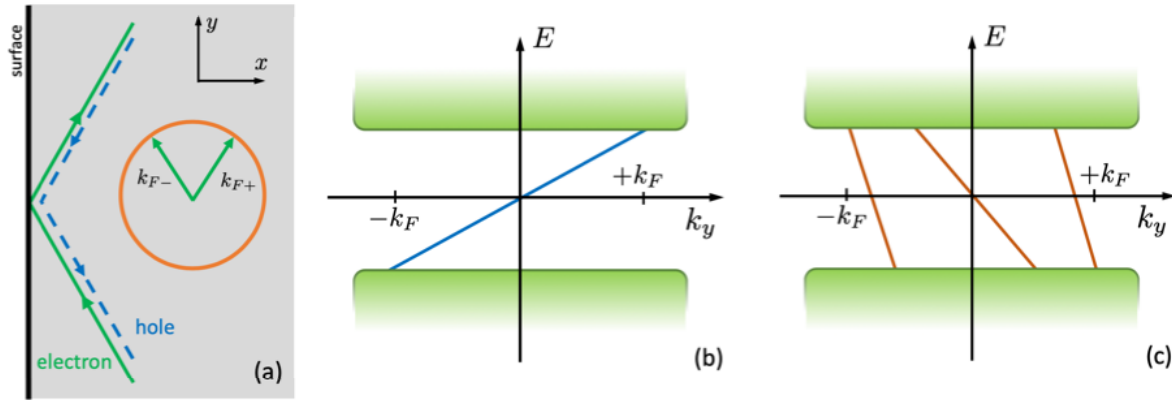


**Fig. 4:** Chiral edge states: (a) Closed quasi-classical trajectories of electrons (green) and holes (blue) connected through Andreev reflections yield subgap bound states at the surface. Schematic structure of the quasiparticle spectrum: (b) Chiral edge mode with energies below the quasiparticle continuum (green) for  $N_C = +1$  [situation as in Fig. 2 (a) and 3 (a) FS 1]. (c) Chiral edge modes for  $N_C = -3$  [situation as shown in Fig. 3 (a) FS 2].

find that  $u_{\mathbf{k}_F}(\mathbf{r}) = u_{\mathbf{k}_F}(\mathbf{r})^* = v_{\mathbf{k}_F}(\mathbf{r}) = v_{\mathbf{k}_F}(\mathbf{r})^*$ . Thus, the creation and annihilation operators are identical  $\hat{\gamma}_0 = \hat{\gamma}_0^\dagger$ . This mode has no electrical charge as electron and hole compensate perfectly. This mode has then the property of a Majorana fermion [12, 13].

Taking  $\Delta_{\mathbf{k}_F} = d_z(\mathbf{k}_F)$  from Eq. (20) we find for the subgap energies

$$E_{k_y} = \pm \Delta_0 \sin k_y \quad (42)$$

which yields a chiral mode whose orientation is connected directly with the chirality, i.e., the sign of the slope corresponds to sign of the Chern number  $N_C$  (see Fig. 4 (b)). The number of surface modes crossing zero energy in with a certain orientation is connected with  $r_{\mathbf{k}_F} = \exp[-i \arg\{d_z(\mathbf{k}_F)\}]$  in Eq. (39) which provides a direct relation to the Chern number in Eq. (25). The Chern number as a winding number determines the number of chiral branches which connect the lower with the upper continuum of the spectrum of Bogoliubov quasiparticles as can be seen upon examination of Eq. (39) [17]. This means eventually,

$$N_C = \sum_{k_y} \text{sign}[v_y(k_y)] \delta(E_{k_y}) \quad (43)$$

where  $N_C$  corresponds to the net number of zero-energy crossings of given sign of velocity  $\hbar v_y(k_y) = dE_{k_y}/dk_y$ . The relation constitutes the concept *bulk-edge correspondence* and shows that the character of the surface bound states are related to the topological properties of the bulk state. This is analogous to the integer Quantum Hall state, for our chiral  $p$ -phase the  $\nu=1$  case. It is instructive to look at the quasi-classical trajectories as displayed in Fig. 4 (a). An electron with given momentum bounces off specularly from the surface back towards the bulk superconductor and is through an Andreev reflection turned into hole which essentially retraces the original path of the electron. With the Andreev reflection of the hole the path is completed

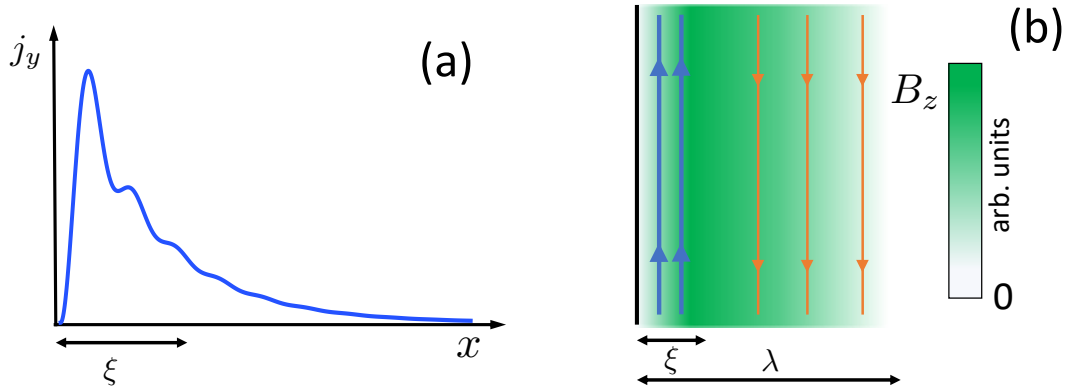


**Fig. 5:** *Spontaneous supercurrent at surface. (a) Charge currents induced by the chiral edge state extend on a length  $\xi$  (coherence length) into the bulk (oscillations are of Friedel-type with wave vector  $k_F$ ). (b) The magnetic field (green shading) induced by the edge current (blue) is screened by counter currents (red) on a length scale  $\lambda$ , the London penetration depth.*

such that we can view this as closed orbit involving both an electron and a hole component, obviously as an electron-hole superposition constituting Bogoliubov quasiparticles as of the superconductor. The localization length along the  $x$ -axis is the order of the bulk coherence length  $\xi \approx \hbar v_F / |\Delta_0|$  as obtained from the wave function in Eq. (37). In the following we will consider the phenomenological implications.

## 4.2 Surface currents

Fig. 4 (a) reveals a further property of the chiral edge state. The closed quasi-classical trajectory for a given  $k_{Fy}$  carries a net electrical current parallel to the surface, because electrons and holes move in opposite direction. Restricting to the Andreev bound states the expression for the current density is given by

$$\begin{aligned}
 J_y(x) &= -\frac{2e}{L} \sum_{k_y = \mathbf{k}_F \cdot \hat{\mathbf{y}}} v_{Fy} \left( |u_{\mathbf{k}_F}(x)|^2 f(E_{k_y}) - |v_{\mathbf{k}_F}(x)|^2 f(-E_{k_y}) \right) \\
 &= -\frac{2e}{L} \sum_{k_y} v_{Fy} \left( |u_{\mathbf{k}_F}(x)|^2 + |v_{\mathbf{k}_F}(x)|^2 \right) f(E_{k_y})
 \end{aligned} \tag{44}$$

with  $\hbar v_F = \nabla_{\mathbf{k}} \xi_{\mathbf{k}} \big|_{\mathbf{k}=\mathbf{k}_F}$ . By symmetry the current density has only a non-vanishing  $y$ -component. The relations  $E_{k_y} = -E_{-k_y}$  and  $v_{Fy}(k_y) = -v_{Fy}(-k_y)$  ensure that the electronic ( $u_{\mathbf{k}}$ ) and hole ( $v_{\mathbf{k}}$ ) part add up in the same direction. Like the bound state this current is confined to a coherence length  $\xi$  at the surface, as shown in Fig. 5. The magnetic field generated by this current is screened (Meissner-Ochsenfeld effect) by counter currents on a length scale of London penetration depth  $\lambda$ , such that the integrated current at the surface vanishes (see Fig. 5(b)). The current induced by the edge states depends on details of the band structure through  $v_F$ . Moreover, it is important to note that also the quasiparticles of the continuum contribute to the current, which lead to some quantitative changes and are ignored in Eq. (44). Consequently, the magnitude of

the current is not uniquely connected with the topology of the chiral state. In contrast to the Quantum Hall state where the chiral edge mode is made up of electrons, here it is a part of the Bogoliubov quasiparticle spectrum. Bogoliubov quasiparticles are due to the hybridization of electrons and holes and, consequently, do not conserve charge [18–20]. As we will show below there is no connection to the Chern number sometimes even not on qualitative level.

It has been discussed whether the chirality would yield a spontaneous Hall effect, a transverse voltage as response to a supercurrent. The discussion of this phenomenon is rather complex and exceeds our analysis. The effect is very small and we refer to Ref. [21].

### 4.3 Quasiparticle current and thermal Hall effect

The analogy to the Quantum Hall effect, however, seems to hold for the Bogoliubov quasiparticles, whose spectrum and current is uniquely connected to the topology of the state. Unlike the charge, the energy of quasiparticles is conserved and we can consider the energy (heat) current carried by the edge states, as defined by

$$J_y^{(Q)}(x) = \frac{1}{L} \sum_{k_{Fy}} E_{k_{Fy}} v_{k_y} \left( |u_{\mathbf{k}_F}(\mathbf{r})|^2 + |v_{\mathbf{k}_F}(\mathbf{r})|^2 \right) f(E_{k_{Fy}}) \quad (45)$$

where the quasiparticle velocity is given by  $\hbar v_y(k_y) = \partial E_{k_y} / \partial k_y$ . Integrating over  $x$  with the normalization condition (38) we obtain

$$I^{(Q)}(T) = \int \frac{dk_y}{2\pi} E_{k_y} v_y(k_y) f(E_{k_y}). \quad (46)$$

In the low-temperature limit ( $k_B T \ll \Delta_0 \sim k_B T_c$ ) we may use Sommerfeld expansion for the temperature dependence

$$\begin{aligned} I^{(Q)}(T) &= \int \frac{dk_y}{2\pi} v_y(k_y) \left( E_{k_y} \Theta(-E_{k_y}) - k_B T \frac{\beta^2 E_{k_y}^2}{4 \cosh^2(\beta E_{k_y}/2)} + \dots \right) \\ &\approx I_0^{(Q)} - \frac{k_B T}{\hbar} \int \frac{dE}{2\pi} \frac{\beta^2 E^2}{4 \cosh^2(\beta E/2)} = I_0^{(Q)} - \frac{\pi}{6} \frac{(k_B T)^2}{\hbar}. \end{aligned} \quad (47)$$

Thus, the first correction to the (non-universal) zero-temperature current is universal, as it does not contain any material-dependent parameters.

Let us now consider a Hall-bar geometry, shown in Fig. 6, where the two edges have by symmetry opposite quasiparticle currents. Due the gap of the bulk state, the electronic heat current is carried only by the edge states. Therefore, the total heat current along the bar consists of the contribution of both surface which flow in opposite direction. A finite current only appears, if the temperature is different on the two surfaces and the leading contribution is

$$I_{tot}^{(Q)} = I_1^{(Q)} + I_2^{(Q)} = \frac{\pi k_B^2}{6 \hbar} (T_2^2 - T_1^2) = -\frac{\pi k_B^2 T}{6 \hbar} \Delta T = \kappa_{yx} \Delta T \quad (48)$$

with  $T_1 = T - \Delta T/2$  and  $T_2 = T + \Delta T/2$ . This is the Righi-Leduc effect, the heat current

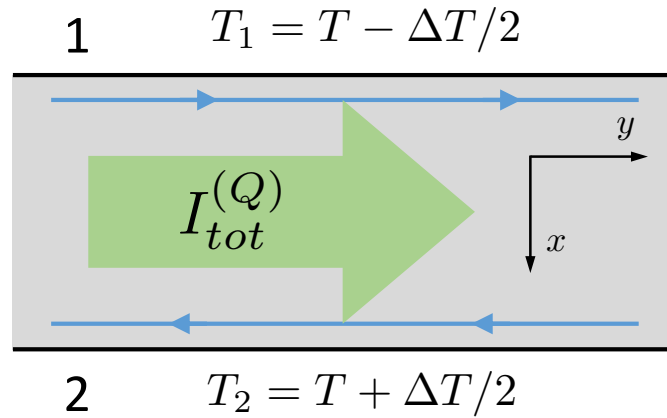


**Fig. 6:** Hall bar for the Righi-Leduc effect or thermal Hall effect: Difference in temperature on the two edges induce a heat current along the bar. For chiral edge states this yields a quantum thermal Hall effect.

induced by a transverse temperature difference is *quantized* with the same universal contribution for each chiral edge mode [14, 22–24], such that we can write

$$\kappa_{xy} = -\kappa_{yx} = \frac{\pi}{6} \frac{k_B^2 T}{\hbar} N_C. \quad (49)$$

Thus, assuming positive chirality ( $k_x + ik_y$ ) for the case in Fig. 3(a) the FS 1 and 2 would yield  $N_C=2$  and  $N_C=-6$ , respectively, including the spin. Note that the universal linear- $T$  behavior is valid only in the limit of very small  $T$  and the leading correction  $\sim e^{-\Delta_0/k_B T} (\Delta_0/k_B T)^2$  is due to thermally activated quasiparticles.

The thermal Hall effect reveals the topological nature of the superconducting phases while neither the spontaneous supercurrent at the surface nor the spontaneous Hall effect are universal and may even be too small to measure. An illustrative example for this discrepancy can be seen in the behavior when crossing the Lifshitz transition for the situation of Fig. 2 (a-c). The spectra of the surface bound states are shown in Fig. 7 (a) and (b) where the former corresponds to the electron-like and the latter to the hole-like Fermi surface. In both cases the Fermi velocity  $v_{Fy}$  entering the surface current expression in Eq. (44) has the same sign for negative energies  $E_{k_y}$ . Thus, in both cases the surface current  $I$  runs in the same direction despite the fact that the two situations correspond to Chern numbers of opposite sign. Thus, the Lifshitz transition between two FS topologies upon rising  $\mu$  leaves at most a slight anomaly in the supercurrent as function of  $\mu$ . The surface current is not tied to the Chern number, but changes sign under the time reversal operation. In contrast, the thermal Hall conductance  $\kappa_{xy}/T$  changes from one universal value to the other, as the quasiparticle velocity  $v_y$  changes sign for the two kinds of edge states.

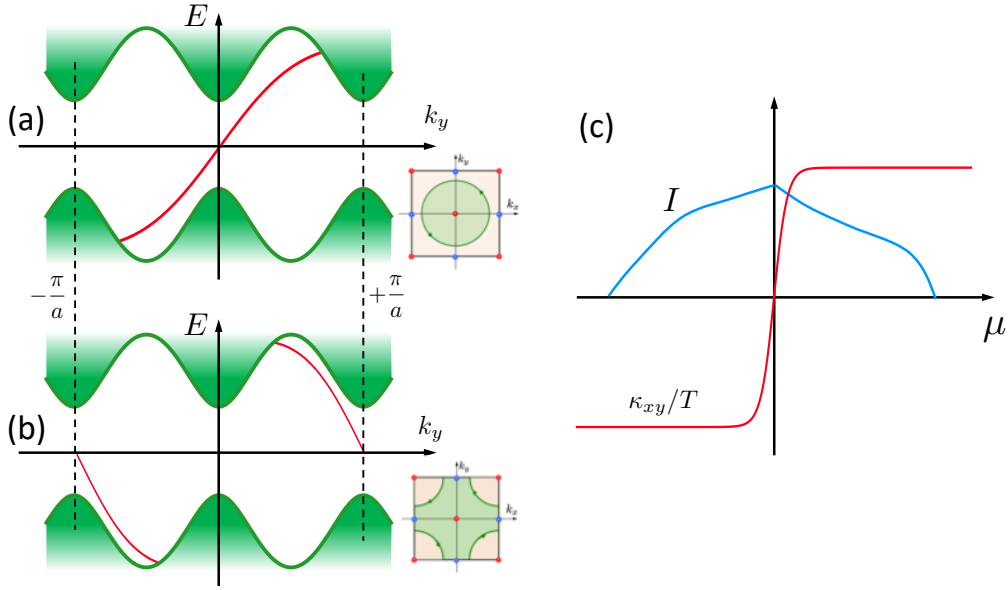


**Fig. 7:** *Topology versus currents: Chiral edge states for (a) electron-like and (b) hole-like FS have dispersions with opposite velocity. (c) The direction of the charge current (electron – hole flow) is unchanged (only small anomaly at the Lifshitz transition at  $\mu = 0$ ), while the thermal Hall conductance  $\kappa_{xy}/T$  changes sign between two universal values (width of the transition shrinks with lowering  $T$ ).*

## 5 Chiral superconductivity in three dimensions

In a genuinely three-dimensional material the generic case of a chiral superconductor is not topologically non-trivial because it has to have zero nodes in the gap. We would like to consider here in a simple way, how one can characterize the properties of such superconductors nevertheless, using some of the tools introduced above.

For our discussion we use again a system with simple tetragonal point group  $D_{4h}$  with a gap function of chiral  $p$ -wave state,  $\mathbf{d}(\mathbf{k}) = \Delta_0 \hat{z}(\sin k_x \pm i \sin k_y)$  without any  $k_z$ -dependence. The chiral axis is along the  $z$ -axis. We now define a sliced Chern number (SCN) by cutting through the three-dimensional BZ for fixed  $k_z$ . The cross section includes again 2D FS ( $\text{FS}(k_z)$ ) which allow us to determine a Chern number through the winding number

$$n_C(k_z) = \frac{1}{2\pi} \oint_{\text{FS}(k_z)} d\mathbf{k} \cdot \nabla_{\mathbf{k}} \arg[d_z(\mathbf{k})] \quad (50)$$

which is an integer and depends on the charges of the encircled gap zero lines crossing the BZ (along  $z$ -direction). The overall ‘‘Chern number’’ is then obtained through the integration over  $k_z$

$$N_C = \frac{a}{2\pi} \int_{-\pi/a}^{+\pi/a} \frac{dk_z}{2\pi} n_C(k_z) . \quad (51)$$

Now let us look at two generic examples, shown in Fig. 8. For a weak dispersion along the  $z$ -

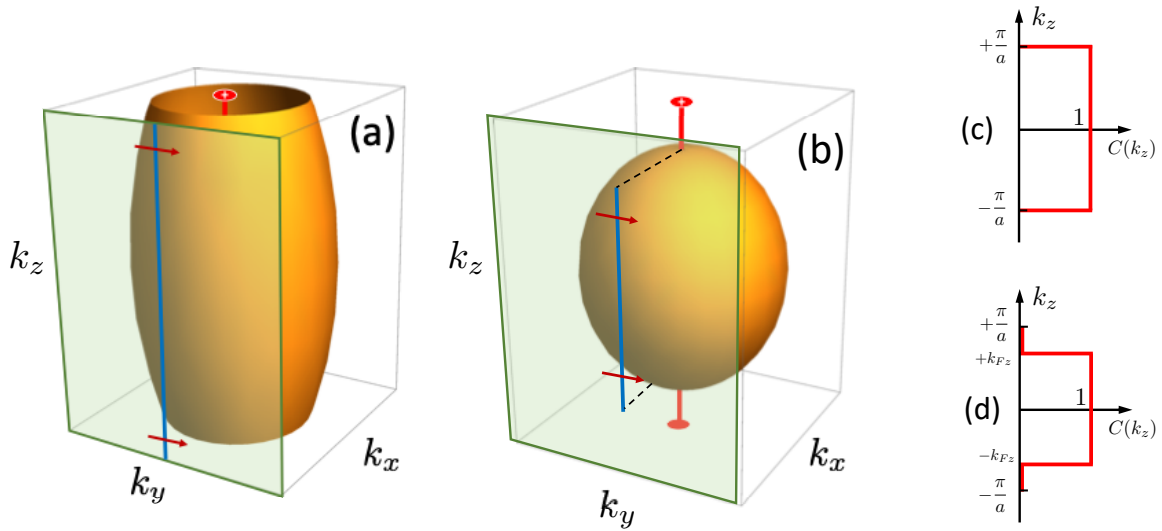


**Fig. 8:** Fermi surfaces in three-dimensional systems: (a) Quasi-two-dimensional metal with open (cylindrical) FS and no gap zeros yields an integer Chern number with a Fermi arc (blue line) crossing the whole surface BZ (green  $k_y$ - $k_z$ -plane). (b) Genuine three-dimensional metal with closed Fermi surface has point nodes at the poles. The Fermi arc is limited by the projection of the nodal points and the non-integer Chern number reflects the restricted length.

axis the FS will be open and cylindrical (a) such that none of the zeros of the gap function  $d_z(\mathbf{k})$  crosses the FS anywhere. This corresponds to a quasi-two-dimensional system. Thus, the bulk quasiparticle spectrum remains fully gapped and  $n_C(k_z) = \pm 1$  for all  $k_z$  in the BZ, as shown in Fig. 8 (c) leading to  $N_C = \pm 1$ , an integer number indicating a topologically non-trivial state. On the other hand, a strong dispersion along the  $z$ -axis yields a closed Fermi surface (Fig. 8 (b)). There are only cross section of the Fermi surface for  $-k_{Fz} < k_z < +k_{Fz}$  where  $n_C(k_z) = \pm 1$ . Here the gap function  $d_z(\mathbf{k})$  has point nodes in the gap at the two poles of the FS ( $k_x = k_y = 0$ ). The Chern number is  $N_C = \pm k_{Fz}a/\pi$ , i.e., non-integer.

What information does the Chern number  $N_C$  carry? These superconductors have chiral edge states connected with  $n_C(k_z)$ , whose spectrum looks as depicted in Fig. 4(b), for a surface with normal vector along  $x$ -direction. For the standard chiral  $p$ -wave state we can find for all  $k_z$  with  $n_C(k_z) = \pm 1$  that there is one  $k_y$  value where  $E_{k_y} = 0$  which we may call a Fermi point. The sign of the sliced Chern number  $n_C(k_z)$  gives these Fermi points an orientation. In the  $k_y$ - $k_z$ -plane they form a so-called Fermi arc which in case (a) crosses the whole BZ while it has a finite length for case (b). The Chern number  $N_C$  is a measure for the length of the Fermi arc. The Chern number  $N_C$  appears again in the thermal Hall effect,

$$\kappa_{xy} = \frac{\pi}{6} \frac{k_B^2 T}{\hbar} \int \frac{dk_z}{2\pi} n_C(k_z) = \frac{\pi}{6} \frac{k_B^2 T}{\hbar} N_C. \quad (52)$$

A universally quantized value is only found for truly topological phases as for the quasi-two-dimensional case (a) in Fig. 8. Note that for the case (b) the presence of point nodes in the gap introduces stronger corrections to linear- $T$  law of  $\kappa_{xy}$  which has a  $T^3$  dependence.

## 6 Topological superconducting phases with TRS

Another class of topological superconductors conserves time reversal symmetry and belong to the odd-parity pairing states, as long as parity is a symmetry. In many aspects these superconductors are related to the B-phase of superfluid  $^3\text{He}$ .

### 6.1 Two-dimensional systems

We return to two-dimensional superconductors and consider here as an example the spin-triplet superconducting phase belonging to one-dimensional representation of the tetragonal point group  $D_{4h}$ . These are given by the gap functions

$$\begin{aligned} \mathbf{d}_{A_{1u}}(\mathbf{k}) &= \Delta_0(\hat{\mathbf{x}} \sin k_x + \hat{\mathbf{y}} \sin k_y), & \mathbf{d}_{A_{2u}}(\mathbf{k}) &= \Delta_0(\hat{\mathbf{x}} \sin k_y - \hat{\mathbf{y}} \sin k_x), \\ \mathbf{d}_{B_{1u}}(\mathbf{k}) &= \Delta_0(\hat{\mathbf{x}} \sin k_x - \hat{\mathbf{y}} \sin k_y), & \mathbf{d}_{B_{2u}}(\mathbf{k}) &= \Delta_0(\hat{\mathbf{x}} \sin k_y + \hat{\mathbf{y}} \sin k_x). \end{aligned} \quad (53)$$

All four states (53) are equal-spin pairing states with spin parallel / antiparallel to the  $z$ -axis. We focus here on  $\mathbf{d}_{A_{1u}}(\mathbf{k})$  which has the following gap matrix

$$\hat{\Delta}_{\mathbf{k}} = \begin{pmatrix} \Delta_{\mathbf{k}\uparrow\uparrow} & \Delta_{\mathbf{k}\uparrow\downarrow} \\ \Delta_{\mathbf{k}\downarrow\uparrow} & \Delta_{\mathbf{k}\downarrow\downarrow} \end{pmatrix} = \begin{pmatrix} -\Delta_0(\sin k_x - i \sin k_y) & 0 \\ 0 & \Delta_0(\sin k_x + i \sin k_y) \end{pmatrix} \quad (54)$$

such that the Nambu space can again be decomposed into two subspace with the spinors  $(\hat{c}_{\mathbf{k}s}, \hat{c}_{-\mathbf{k}s})$  with  $s = \pm 1$  for spin up and down, respectively. It is obvious that each subspace has a ‘‘chiral’’ gap function with a definite ‘‘Chern number’’

$$N_{C,s} = \frac{1}{2\pi} \oint_F S d\mathbf{k} \cdot \nabla_{\mathbf{k}} \arg[\Delta_{\mathbf{k}ss}] \quad (55)$$

which is spin dependent with  $N_{C,+1} = -N_{C,-1}$ . The net Chern number taking both spins together,  $N_C = \sum_s N_{C,s} = 0$ , vanishes, since TRS is conserved. Nevertheless, bulk-edge correspondence is reflected by the presence of ‘‘spin chiral edge states’’ of opposite orientation for the two spin subspaces (see Fig. 9(a)):  $E_{k_y,s} = \text{Im}[\Delta_{\mathbf{k}_F,ss}]$ . These edge states can be obtained again by means of the Bogoliubov-de Gennes equations used above. They are called *helical* as propagation direction and spin of the quasiparticles are tied together.

Analogous to Sect. 4.1 we introduce again quasiparticle operators for the edge state which have now a spin index,  $\hat{I}_{k_y} = (\hat{\gamma}_{k_y\uparrow}, \hat{\gamma}_{k_y\downarrow})$ . The surface Hamiltonian reads,

$$\mathcal{H}_{\text{sf}} = \sum_{k_y,s} E_{k_y,s} \hat{\gamma}_{k_y,s}^\dagger \hat{\gamma}_{k_y,s} = \sum_{k_y,s,s'} \mathcal{E}_{k_y,ss'} \hat{\gamma}_{k_y,s}^\dagger \hat{\gamma}_{k_y,s'} \quad (56)$$

Here  $\mathcal{E}_{k_y,ss'}$  follows from the symmetry general relation  $(\hat{\mathbf{n}} \times \mathbf{k}_{\parallel}) \cdot \boldsymbol{\sigma}_{ss'} = k_y \sigma_{ss'}^z$  where  $\hat{\mathbf{n}} = (100)$  is the surface normal vector and  $\mathbf{k}_{\parallel}$  the momentum parallel to the surface.

For the time being we restrict here to the situation of an electron like FS closed around the BZ center, for simplicity.

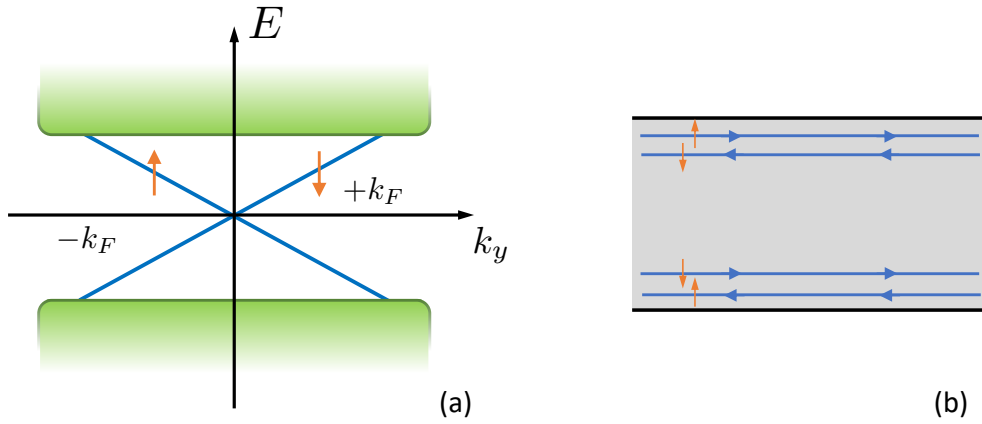


**Fig. 9:** Helical edge states: (a) The energy dispersion is spin dependent with opposite quasi-particle velocity for up and down spin. (b) This yields spin currents at the surface.

## 6.2 Surface currents and universal properties

Due to TRS conservation there is no spontaneous supercurrent along the surface unlike in the case of a chiral superconducting phase. The helical spectrum of the Andreev bound states results in a spin current in turn. Following the same way as in Eq. (44) we find that after the integration over  $x$  the total surface current for the spin  $s$  is given by

$$I_{y,s} = \frac{1}{L} \sum_{k_y} v_{Fy}(k_y) f(E_{k_y,s}). \quad (57)$$

With the relations,  $E_{k_y,s} = -E_{k_y,\bar{s}} = E_{-k_y,\bar{s}}$  and  $v_{Fy}(k_y) = -v_{Fy}(-k_y)$  follows that  $I_{y,s} = -I_{y,\bar{s}}$ . Therefore obviously the supercurrent vanishes, i.e.,  $I_y = I_{y,\uparrow} + I_{y,\downarrow} = 0$ . However, we obtain a net spin current along the edge

$$I_y^{(s)} = \frac{\hbar}{2} (I_{y,\uparrow} - I_{y,\downarrow}) = \frac{\hbar}{L} \sum_{k_y} v_{Fy}(k_y) f(E_{k_y,\uparrow}) \quad (58)$$

whereby this current runs in the opposite direction on the two edges of a bar as shown in Fig. 9(b). This current would also contain contributions from the continuum not included in Eq. (57). Like the chiral supercurrents these spin currents are not universal. Unlike the supercurrent, the spin current does not lead to screening currents.

On the other hand, there is an analog to the quantized thermal Hall effect for chiral superconductors. Very much in the same way as in Sect. 4.3 we can derive a relation like in Eq. (48),

$$\kappa_{xy}^{(s)} = -\kappa_{yx}^{(s)} = \frac{\pi k_B^2 T}{3 \hbar} \quad (59)$$

whereby the response to the transverse temperature difference in the Hall bar is a “spin heat current”

$$I_y^{(Q,s)} = \int \frac{dk_y}{2\pi} E_{k_y} v_y(k_y) (f(E_{k_y,\uparrow}) - f(E_{k_y,\downarrow})). \quad (60)$$

Considering this in a Hall bar geometry again, this would constitute a quantized thermal spin Hall effect. An experimental verification would very likely be rather challenging.

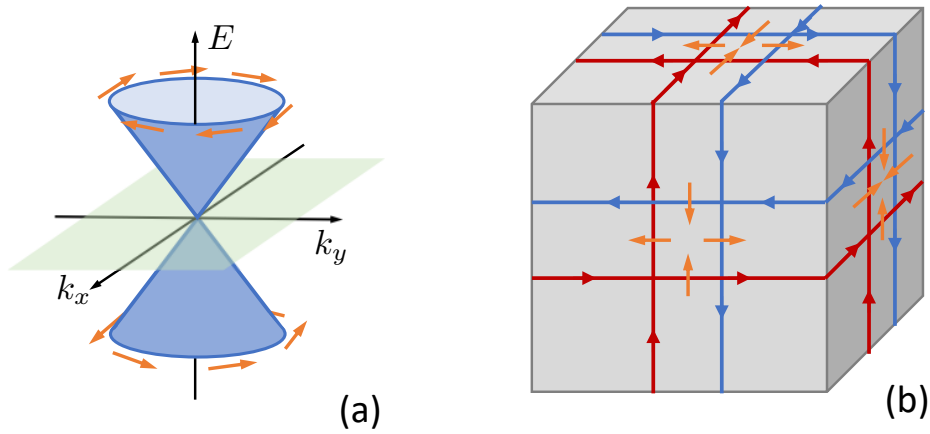


**Fig. 10:** Edge states for the Balian-Werthammer state  $\mathbf{d}(\mathbf{k}) = \Delta_0 \hat{\nu} \cdot \mathbf{k}$ : (a) The edge states are helical with Dirac-type cone dispersion on the two surface BZ (here  $k_x$ - $k_y$ ). The arrows (orange) show the spin texture. (b) These edge states yield spin currents with transverse spin orientation on all surfaces.

### 6.3 Three-dimensional systems

The prime example of a topological phase in this category is the Balian-Werthammer (BW) state which corresponds to the B-phase of superfluid  $^3\text{He}$  [3, 10]. It is an odd-parity state with a gap function

$$\mathbf{d}(\mathbf{k}) = \begin{cases} \Delta_0(\hat{\mathbf{x}}k_x + \hat{\mathbf{y}}k_y + \hat{\mathbf{z}}k_z) & \text{(I)} \\ \Delta_0(\hat{\mathbf{x}} \sin k_x + \hat{\mathbf{y}} \sin k_y + \hat{\mathbf{z}} \sin k_z) & \text{(II)} \end{cases} \quad (61)$$

where case (I) corresponds to a fully rotationally symmetrical system like  $^3\text{He}$  and case (II) is the analogous state in a simple cubic lattice with nearest-neighbor pairing. Unlike all the other odd-parity states considered above this is not an equal-spin pairing state. The spin configuration is locked to the momentum space (like for the states in Eq. (53) which constitutes a dynamical “spin-orbit coupling”). The gap function has no zeros on a closed Fermi surface in case (I) and in case (II) there is a finite number of zero points in the BZ. The analysis of the topology by slicing the BZ reveals that “topological invariants” only exist for  $\mathbf{k} \cdot \hat{\nu} = 0$  ( $\hat{\nu}$  slicing normal vector) or at the BZ boundary for case (II). Thus, we do not have Fermi arcs unlike in the case of time reversal symmetry breaking chiral superconductors.

It is straightforward to derive the edge states from the corresponding Bogoliubov-de Gennes equations [25, 12]. The corresponding surface Hamiltonian for case (I) reads

$$\mathcal{H}_{\text{sf}} = \sum_{\mathbf{k}_{\parallel}, s, s'} (\hat{\mathbf{n}} \times \mathbf{k}_{\parallel}) \cdot \boldsymbol{\sigma}_{ss'} \hat{\gamma}_{\mathbf{k}_{\parallel}, s}^{\dagger} \hat{\gamma}_{\mathbf{k}_{\parallel}, s'} \quad (62)$$

which shows a helical spectrum with a cone shaped dispersion around the center of the surface BZ. In Fig. 10(a) we show the momentum dependence of the subgap quasiparticle energy for the normal vector along the  $z$ -axis. This leads to surface spin currents as displayed in Fig. 10(b). In this case we have only a Fermi point in the surface BZ. In case (II) it is possible to have additional such cones at points of the BZ boundary some of which show a reversed spin pattern.

AZ class	$SU(2)$	TRS	parity	examples	edge states
D	$\times$	$\times$	odd	spinless chiral $p$ -wave	chiral
DIII	$\times$	$\bigcirc$	odd	BW $p$ -wave	helical
A	$\triangle$	$\times$	odd	spinful chiral $p$ -wave	chiral
AIII	$\triangle$	$\bigcirc$	odd	nematic	zero-energy
C	$\bigcirc$	$\times$	even	chiral $d$ -wave	chiral
CI	$\bigcirc$	$\bigcirc$	even	nematic	zero-energy

**Table 1:** Six classes of Bogoliubov-de Gennes Hamiltonians: We distinguish behavior under spin  $SU(2)$  and TRS operation – “ $\bigcirc$ ” present, “ $\times$ ” absent, “ $\triangle$ ” restricted  $SU(2)$  with  $S_z$  preserved. We use examples discussed in parts above.

## 7 Symmetry classification

In the context of topological phases, in particular topological insulators, single-particle Hamiltonians have been categorized into ten symmetry classes and led to the so-called periodic table of topological matter. Among these we find also the classes to which superconductors belong, the subgroup of the Bogoliubov-de Gennes Hamiltonians [26,27]. In this section we would like briefly to locate the examples we have given above within this classification scheme, because it is often used in literature. The basis of the classification are properties of the Hamiltonian as given in Eq. (11) under the discrete symmetries of time-reversal, particle-hole, and sublattice (so-called chiral) symmetry. In Table 1 we give the list of the six relevant classes which are labeled according to the Altland-Zirnbauer (AZ) classes [28].

We will now consider briefly the different classes.

*Classes without spin rotation symmetry  $SU(2)$ :* Class D violating TRS is in 2D systems characterized by an integer Chern number. An example is a spinless chiral  $p$ -wave superconductor, e.g., the reduced Hamiltonian in Eq. (21) which possesses chiral edge states. The class DIII conserves TRS and includes the superconducting states discussed in Sect. 6 which generate helical edge states in two and three dimensions.

*Classes with conserved spin  $S_z$ -component:* We find the spinful chiral  $p$ -wave superconductor including both spin components in  $H(\mathbf{k})$  possessing integer Chern numbers in 2D systems. This belongs to class A without TRS and has chiral edge states. Class AIII with TRS contains the odd-parity states like nematic phase  $B$  and  $C$  in Eq. (9). These states have zeros in the gap. They can develop zero-energy Andreev bound states for certain surfaces as can be seen from our analysis in Sect. 4.1. For all trajectories with  $\Delta_{\mathbf{k}_{F+}} = -\Delta_{\mathbf{k}_{F-}}$  we find from Eq. (39)  $E=0$ .

*Classes with full spin rotation symmetry:* Here we find the even-parity spin-singlet superconductors where Cooper pairs do not have any spin dependence. The class C breaks TRS and incorporates the chiral  $d$ -wave state,  $d_{x^2-y^2} + id_{xy}$ -wave, which is characterized by a Chern number in 2D and possesses chiral edge states. An alternative chiral  $d$ -wave state in 3D systems has  $d_{xz} + id_{yz}$ -symmetry with a line node. Nematic  $d$ -wave states like  $d_{x^2-y^2}$  and  $d_{xy}$  belong to class CI. Analogous to the nematic odd-parity states, they have zero-energy Andreev bound states for certain surface orientations.

## 8 Realizations of topological superconducting phases

As mentioned in the introduction unconventional superconductivity is most likely found in materials with strongly correlated electrons. While such superconductors are known since the late 1970's it is still a highly non-trivial task to identify the structure of Cooper pairs.

A few experimental methods are considered important in the context of topological superconductivity. For the detection of spontaneously broken TRS in superconductors there are two widely trusted methods. These are the zero-field muon spin relaxation (see, e.g., Ref. [29]) and the polar Kerr effect (see, e.g., Ref. [30]). The former measures the depolarization rate of the spins of injected muons. For numerous superconductors we find an increase of the depolarization rate indicating that the superconductor produces intrinsically a spontaneous magnetic field distribution associated with broken TRS. The polar Kerr effect observes the rotation of the polarization axis of reflected light relative to the incident polarization. By symmetry such an effect is possible for chiral superconductors for incident beams along the chiral axis. The estimate of the magnitude of the observed signals, however, is a complex theoretical problem [30].

Among the superconductors labeled as TRS breaking by these two methods, we find several which are candidates for chiral superconductivity. In this respect the most intensively investigated is  $\text{Sr}_2\text{RuO}_4$  which has been suggested to be a chiral  $p$ -wave superconductor [8, 31]. During the last year, however, new experimental data led to a debate whether  $\text{Sr}_2\text{RuO}_4$  is indeed an odd-parity superconductor.  $\text{SrPtAs}$  has been discussed as a candidate for chiral  $d$ -wave superconductivity of the  $d_{x^2-y^2}+id_{xy}$ -wave type [32, 33]. Chiral  $d$ -wave superconductivity of the  $d_{zx}+id_{zy}$ -wave type has been proposed for the heavy Fermion superconductor  $\text{URu}_2\text{Si}_2$  [30, 34]. Chiral superconductivity may also be realized in  $\text{UPt}_3$ , another heavy Fermion compound, as a chiral  $f$ -wave channel, with a gap function,  $\mathbf{d}(\mathbf{k}) = \hat{z}k_z(k_x+ik_y)^2$  or  $\mathbf{d}(\mathbf{k}) = \hat{z}(k_x+ik_y)(5k_z^2-1)$  [35, 36].

While magnetic properties have been observed through  $\mu\text{SR}$  and polar Kerr effect in many of these superconductors, so far attempts, focussed mainly on  $\text{Sr}_2\text{RuO}_4$ , to directly detect the magnetic fields produced by surface currents, using scanning probes, have only delivered negative results [37, 38]. This may reflect the fact that the generated magnetic fields are not universal and too small for the conditions in the experiment [18–20]. On the other hand, quasiparticle tunnelling data for  $\text{Sr}_2\text{RuO}_4$  show zero-bias anomalies indicating the presence of edge states [39, 40]. Note, however, that these experiments cannot distinguish chiral from helical edge states easily.

Since magnetism is considered adversary to superconductivity, the superconducting phases appearing in the ferromagnetic heavy Fermion systems,  $\text{UGe}_2$ ,  $\text{URhGe}$  and  $\text{UCoGe}$ , have attracted also much attention [41, 42]. These systems break TRS even in the normal state and the Cooper pairs form in a spin polarized environment, most likely with odd-parity. This has been the basis of proposals of superconducting phases with topological properties (for a recent work see [43]). A most recent case of an U-based superconductors which possibly realizes chiral pairing is  $\text{UTe}_2$ , a heavy Fermion metal close to a ferromagnetic quantum critical point [44].

Unconventional superconductivity in materials without an inversion center in their crystal lattice

represent another intriguing class, because parity is not a symmetry for Cooper pairs anymore. Also here topological features have been discussed (see for example [45]). A brief overview of the many realizations of topological bulk superconductors can be found in Ref. [46].

## 9 Conclusion

This brief lecture notes give only a very selected insight into a very dynamical and fast evolving field. The very active subject of artificially structured systems designed to show topological superconductivity have been completely omitted. In particular, one-dimensional systems, so-called nano-wires, provide a way to generate Majorana edge modes in a controlled way and are considered as potential building blocks for so-called topological quantum computers [47, 48]. Also nodal structures of the pair wavefunction or the gap functions are a subject of topological matter [49, 50].

## References

- [1] M. Sigrist and K. Ueda, *Rev. Mod. Phys.* **63**, 239 (1991)
- [2] V.P. Mineev and K.V. Samokhin: *Introduction to Unconventional Superconductivity* (Gordon and Breach, 1999)
- [3] A.J. Leggett, *Rev. Mod. Phys.* **47**, 331 (1975)
- [4] G.R. Stewart, *Adv. Phys.* **66**, 75 (2017)
- [5] M.R. Norman, *Science* **332**, 196 (2011)
- [6] C. Pfleiderer, *Rev. Mod. Phys.* **81**, 1551 (2009)
- [7] B.D. White, J.D. Thompson, and M.B. Maple, *Physica C* **514**, 246 (2015)
- [8] Y. Maeno, S. Kittaka, T. Nomura, S. Yonezawa, and K. Ishida, *J. Phys. Soc. Jpn.* **81**, 011009 (2012)
- [9] A.P. Mackenzie, *J. Supercond. Nov. Magn.* **33**, 177 (2020)
- [10] D. Vollhardt and P. Wölfle: *The Superfluid Phases of Helium 3* (Taylor & Francis, 1990)
- [11] X.L. Qo and S.C. Zhang, *Rev. Mod. Phys.* **83**, 1057 (2011)
- [12] B.A. Bernevig and T.L. Hughes: *Topological Insulators and Topological Superconductors* (Princeton University Press, 2013)
- [13] M. Sato and Y. Ando, *Rep. Prog. Phys.* **80**, 076501 (2017)
- [14] N. Read and D. Green, *Phys. Rev. B* **61**, 10267 (2000)
- [15] G.E. Volovik, *Sov. Phys. JETP* **67**, 1804 (1988); *JETP Lett.* **66**, 522 (1997)
- [16] J.B. Ketterson and S.N. Song: *Superconductivity* (Cambridge University Press, 1999)
- [17] G.E. Volovik and V.M. Yakovenko, *J. Phys.: Condens. Matter* **1**, 5263 (1989)
- [18] W. Huang, E. Taylor, and C. Kallin, *Phys. Rev. B* **90**, 224519 (2014)
- [19] S. Lederer, W. Huang, E. Taylor, S. Raghu, and C. Kallin, *Phys. Rev. B* **90**, 134521 (2014)
- [20] S.B. Etter, A. Bouhon, and M. Sigrist, *Phys. Rev. B* **97**, 064510 (2018)
- [21] A. Furusaki, M. Matsumoto, and M. Sigrist, *Phys. Rev. B* **64**, 054514 (2001)
- [22] T. Qin, Q. Niu and J. Shi, *Phys. Rev. Lett.* **107**, 236601 (2011)
- [23] H. Sumiyoshi and S. Fujimoto, *J. Phys. Soc. Jpn.* **82**, 023602 (2013)

- [24] Y. Imai, K. Wakabayashi, and M. Sigrist, *Phys. Rev. B* **93**, 024510 (2016)
- [25] Y. Okuda and R. Nomura, *J. Phys.: Condens. Matter* **24**, 343201 (2012)
- [26] A.P. Schnyder, S. Ryu, A. Furusaki, and A.W.W. Ludwig, *Phys. Rev. B* **78**, 195125 (2008)
- [27] C.K. Chiu, J.C.Y. Teo, A.P. Schnyder, and S. Ryu, *Rev. Mod. Phys.* **88**, 035005 (2016)
- [28] A. Altland und M.R. Zirnbauer, *Phys. Rev. B* **55**, 1142 (1997)
- [29] G.M. Luke, Y. Fudamoto, K.M. Kojima, M.I. Larkin, J. Merrin, B. Nachumi, Y.J. Uemura, Y. Maeno, Z.Q. Mao, Y. Mori, H. Nakamura, and M. Sigrist, *Nature* **394**, 558 (1998)
- [30] A. Kapitulnik, *Physica B* **460**, 151 (2015); E.R. Schemm, E.M. Levenson-Falk, and A. Kapitulnik, *Physica C* **535**, 13 (2017)
- [31] Y. Liu and Z.Q. Mao, *Physica C* **514**, 339 (2015)
- [32] P.K. Biswas, H. Luetkens, T. Neupert, T. Stürzer, C. Baines, G. Pascua, A.P. Schnyder, M.H. Fischer, J. Goryo, M.R. Lees, H. Maeter, F. Brückner, H.-H. Klauss, M. Nicklas, P.J. Baker, A.D. Hillier, M. Sigrist, A. Amato, and D. Johrendt *Phys. Rev. B* **87**, 180503 (2013)
- [33] M.H. Fischer, T. Neupert, C. Platt, A.P. Schnyder, W. Hanke, J. Goryo, R. Thomale, and M. Sigrist, *Phys. Rev. B* **89**, 020509 (2014)
- [34] Y. Kasahara, T. Iwasawa, H. Shishido, T. Shibauchi, K. Behnia, Y. Haga, T.D. Matsuda, Y. Onuki, M. Sigrist, and Y. Matsuda, *Phys. Rev. Lett.* **99**, 116402 (2007)
- [35] E.R. Schemm, W.J. Gannon, C.M. Wishne, W.P. Halperin, and A. Kapitulnik, *Science* **345**, 190 (2014)
- [36] P. Goswami and A.H. Nevidomskyy, *Phys. Rev. B* **92**, 214504 (2015)
- [37] J.R. Kirtley, C. Kallin, C.W. Hicks, E.-A. Kim, Y. Liu, K.A. Moler, Y. Maeno, and K.D. Nelson, *Phys. Rev. B* **765**, 014526 (2007)
- [38] P.J. Curran, S.J. Bending, W.M. Desoky, A.S. Gibbs, S.L. Lee, and A.P. Mackenzie, *Phys. Rev. B* **89**, 144504 (2014)
- [39] Z.Q. Mao K.D. Nelson, R. Jin, Y. Liu, and Y. Maeno, *Phys. Rev. Lett.* **87**, 037003 (2001)
- [40] S. Kashiwaya, H. Kashiwaya, H. Kambara, T. Furuta, H. Yaguchi, Y. Tanaka, and Y. Maeno, *Phys. Rev. Lett.* **107**, 077003 (2011)
- [41] A.D. Huxley, *Physica C* **514**, 368 (2015)
- [42] D. Aoki, K. Ishida, and J. Flouquet, *J. Phys. Soc. Jpn.* **88**, 022001 (2019)

- 
- [43] A.K.C. Cheung and S. Raghu, *Phys. Rev.* **93**, 134516 (2016)
  - [44] L. Jiao, S. Howard, S. Ran, Z. Wang, J. Olivares Rodriguez, M. Sigrist, Z. Wang, N.P. Butch, and V. Madhavan, *Nature* **579**, 523 (2020)
  - [45] M. Sato and S. Fujimoto, *Phys. Rev. B* **79**, 094504 (2009)
  - [46] S. Yonezawa, *AAPPS Bulletin* **26**, No. 3, 3 (2016)
  - [47] M. Franz, *Nat. Nanotechnol.* **8**, 149 (2013)
  - [48] H.M. Guo, *Sci. China-Phys. Mech. Astron.* **59**, 637401 (2016)
  - [49] S. Kobayashi, Y. Yanase, and M. Sato, *Phys. Rev. B* **94**, 134512 (2016)
  - [50] T. Bzdusek and M. Sigrist, *Phys. Rev. B* **96**, 155105 (2017)

